Analyst

TUTORIAL REVIEW

View Article Online
View Journal | View Issue

Cite this: *Analyst*, 2026, **151**, 1597

Recent developments in micro- and nanofluidic catalytic reactors utilizing ultra-small spaces

Ben-Yuan Zhang, †[a] Koki Yamamoto, †[b] Po-Yen Chen [a] and Kyojiro Morikawa *[a,c,d]

Microfluidics and nanofluidics have contributed much to the fields of chemistry and biochemistry. The small sizes of micro and nanochannels provide short diffusion lengths, resulting in highly efficient reactions with control over channel size, flow and temperature. In this review, progress in chemical and biochemical reactors based on micro and nanochannels is summarized. Various types of reactors such as homogeneous and heterogeneous catalytic reactors based on wall-coated, packed-bed or monolithic column designs are examined. The ultra-small spaces provided by micro and nanochannels allow rapid mixing and promote interactions between different phases. As such, faster reaction rates and better yields can be obtained using systems that are easy to operate. In addition, unique reaction mechanisms can be achieved based on the specific properties exhibited only by nanospaces. Although it remains challenging to balance high efficiency with a suitable production volume, new super-high-performance reactors allowing well-controlled processes with suitable productivity are anticipated in future. This advanced technology will represent significant progress in the areas not only of analytical chemistry and bioanalytical chemistry, but also chemical and biochemical engineering.

Received 29th November 2025,
Accepted 18th February 2026

DOI: 10.1039/d5an01253h

rsc.li/analyst

1. Introduction

Recent advances in microfluidics[1–3] and nanofluidics[4–6] have greatly contributed to the fields of chemistry and biochemistry. These technologies are unique because the small dimensions of micro and nanochannels provide short diffusion lengths. Typically, microchannels have characteristic widths, depths, or diameters ranging from 1 to 1000 μm, whereas nanochannels have corresponding dimensions on the order of 1–1000 nm. In contrast to bulk-scale systems, this allows the rapid mixing of different liquid phases and promotes interactions between the surface/liquid interface and the liquid phase by providing a high surface-to-volume (S/V) ratio. Uniform solute concentrations and flow conditions can also be achieved. In addition, the minute sample volumes in micro and nanochannels permit rapid heat transfer, allowing precise control over the liquid temperature. Hence, these ultra-small spaces can modify the primary factors controlling chemical reactions, such as solute concentration, reaction time and temperature.

For the purpose of controlling these parameters, it is vital to precisely adjust the channel sizes. Many methods for the fabrication of micro and nanochannels have been developed, primarily using materials such as polydimethylsiloxane (PDMS),[7–9] SU-8,[10,11] poly(methyl methacrylate)[12,13] and polyethylene terephthalate.[14,15] It is often important for these materials to withstand high temperatures and pressures and to tolerate contact with organic solvents. Glass is typically the most suitable material meeting these requirements and also permits visual observations and surface modifications. The fabrication of channels using glass substrates is relatively difficult, but technologies for the production of glass nanochannels[16–20] and microchannels[21–25] have been developed. In addition, flow control methods[26–29] for adjusting concentrations, reaction times (that is, liquid passage durations) and temperature[30–32] in micro or nanofluidic devices have all been reported. Such technologies provide a foundation for highly-controlled reaction processes. The volumes of microfluidic devices are typically in the nL to μL range, resulting in minimized sample consumption and waste generation. In contrast, nanofluidic systems operate at much smaller volumes, typically in the fL to pL range. Such ultra-small volumes have enabled analytical capabilities that are difficult or impossible to achieve in bulk systems, including single-cell[33–35] and

[a]*Institute of NanoEngineering and MicroSystems, Department of Power Mechanical Engineering, National Tsing Hua University, Hsinchu, Taiwan.*
E-mail: morikawa@pme.nthu.edu.tw
[b]*Center for Biosystems Dynamics Research, RIKEN, Kobe, Japan*
[c]*Collaborative Research Organization for Micro and Nano Multifunctional Devices, The University of Tokyo, Tokyo, Japan*
[d]*Kanagawa Institute of Industrial Science and Technology, Kanagawa, Japan*
†These authors contributed equally.

single-molecule analyses. Owing to these characteristics, micro- and nanofluidic techniques have been widely adopted in the fields of analytical and bioanalytical chemistry.

While micro- and nanofluidic reactors are advantageous for precise reaction control and the minimization of sample consumption, they inherently limit throughput and productivity, which are critical for practical chemical and biochemical processes. However, when these systems are interfaced with conventional analytical instruments that typically require sample volumes in the μL to mL range, such extremely small reaction volumes become a significant limitation. This is because reducing the reaction volume decreases the absolute amount of target analyte and solution available for analysis. As a result, there is a trade-off between good reaction control and productivity. Therefore, the central challenge in micro- and nanofluidics lies in reconciling precise reaction control with scalable production depending on the specific application and design context.

This review introduces and organizes recent advances in the use of micro and nanochannels providing ultra-small spaces to promote various reactions. For this aim, mainly two kinds of approaches are shown in this review. One is the scale-down method by packing with micro and/or nano structures, which provides μL to mL reaction volume, but size control is difficult. The other is the numbering-up method of the size-regulated channels, which provides good reaction control, but productivity is still a challenge. The utilization of these devices with the trade-off between reaction efficiency and productivity is discussed, especially with regard to production at higher volumes. Catalytic reactors with applications to chemical and biochemical processes based on micro or nanofluidics are introduced, with a focus on the combination of ultra-small spaces with catalysts.

2. Microfluidic and nanofluidic biomolecular reactors

A bioreactor is a device in which biological processes such as reactions, syntheses, decompositions and transformations occur. These systems are designed to use biological substrates such as microorganisms, cells and enzymes[36–38] and typically permit control over physical and chemical parameters such as temperature, pressure, pH, solvent and enzyme supply. Tuning the design and operation of a bioreactor is a crucial aspect of optimizing the conditions for specific processes and maximizing yields and efficiency. Recently, micro and nanofluidic bioreactors have attracted attention with regard to analytical, biological and industrial applications along with the development of micro and nanofabrication technologies.[39–41] Specifically, the reaction volume, reaction velocity and mixing ratio can be tuned by controlling the channel size, flow rate and temperature. Moreover, such devices provide several advantages, including rapid heat and mass transfer, efficient mixing, precise control over reaction parameters and minimized sample volumes. The present section examines recent advances in micro and nanofluidic bioreactors, including liquid and solid phase systems (Fig. 1), with a particular focus on channel-based reactors providing well-defined spaces, precise fluid flows and constant temperatures (Table 1).

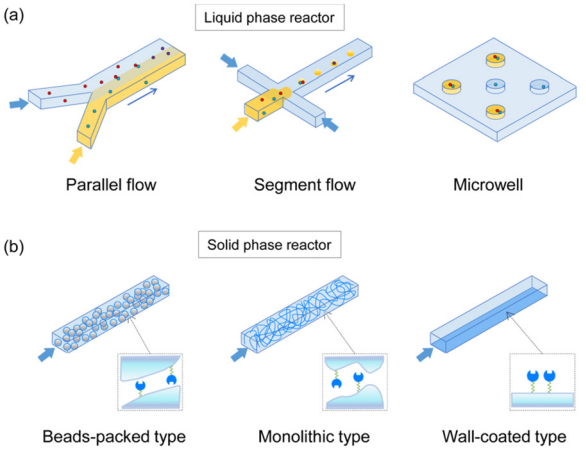

Fig. 1 . (a) Diagrams of several liquid phase bioreactors. Such reactors are primarily categorized as parallel flow, segmented flow or microwell reaction types. (b) Diagrams of solid phase bioreactors. These devices are categorized as packed bead, monolithic or wall-coated types. Enzymes are generally immobilized on the support materials.

2.1 Homogeneous catalysts for biochemical reactors

There are several significant differences between flow-through bioreactors and batch reactions. In a flow-through reaction system, a continuous reactant flow is maintained through the application of external pressure, allowing for controlled reaction times. Notably, micro and nanofluidic systems enable efficient heat and mass transfer based on the extremely small volumes and high S/V ratios in such devices. These systems can be combined with various flow channel and chamber morphologies to generate either parallel flow or segmented (droplet) flow (Fig. 1(a)).[55] The former is characterized by the simultaneous flow of layers comprising different phases whereas, in the latter, a droplet of one phase is dispersed in another phase, which can have various sizes and shapes. These devices permit control over both the reaction time and mixing ratio. Combining these reaction systems can allow micro and nanofluidic bioreactors to facilitate rapid reactions with higher yields and greater productivity compared with conventional batch processes.

Microfluidic bioreactors allow for the effective capture, separation, culturing and analysis of cells based on a serial process. These platforms have thus advanced the techniques available for the analysis of cells, microorganisms and viruses, which can be encapsulated in microfabricated compartments or droplets.[56] The associated methodologies are able to process extremely small samples, such as single cells or even individual molecules. Such systems have the ability to integrate multiple operations using continuous flow in conjunction with rapid heat transfer, such that enzymatic reactions

Table 1 Summary of typical biomolecular reactors

Material	Channel/reactor dimensions	Specific surface area	Reaction time	Productivity	Immobilized enzyme (or free enzyme)	Reaction sample (or substrate)	Highlight	Ref.
Glass capillary	Beads-packed i.d. 250 μm × ~0.7 cm Beads size: 45–165 μm	6.5×10^4–2.4×10^5 m^{-1}	~10 min	~32 nL min^{-1}	Trypsin	α-Synuclein	A fully integrated on-line affinity solid-phase extraction–bead-packed IMER–CE–MS platform enables rapid enzymatic digestion and sensitive bottom-up analysis of α-synuclein.	42
Glass capillary	Monolith i.d. 50 μm × 20 mm Pore size: 0.69–1.08 μm	~2×10^6 m^{-1}	~1 min	~0.5 μL min^{-1}	Trypsin	BODIPY labeled casein Myoglobin	A dual-function SPE–IMER monolith enables rapid digestion and high-coverage bottom-up CE–MS protein analysis.	43,44
Hydrogel in EP tube	Monolith (molecular sieve) Pore size: 10 nm	on the order of 10^8 m^{-1}	~1 min	~100 μL/1 min	Trypsin and Glu-C	Bovine serum albumin (BSA), bovine hemoglobin (BHb)	A hydrophilic dual-enzyme IMER (trypsin/Glu-C) enables ultrafast protein digestion within 1 min with >90% sequence coverage *via* enhanced mass transfer and orthogonal cleavage.	45
Glass	Nanochannel				Trypsin			
	a. w 18 μm × d 300 nm × L 6 mm	a. 3.3 × 10^6 m^{-1}	a. 0.7, 1.5, 3.1, 4.7, 5.8, 7.2, 16 min	a. 2.0, 4.5, 5.6, 6.9, 10, 22, 46 pL min^{-1}		a. BAPNA	a. An enzymatic reaction was 25 times faster than by a conventional bulk method due to the high surface-to-volume ratio	a. 46
	b. w 18 μm × d 300 nm × L 6 mm	b. 3.3 × 10^6 m^{-1}	b. 5, 15, 30, 45, 60 min	b. 0.5, 0.7, 1.1, 2.2, 6.5 pL min^{-1}		b. Cytochrome C	b. An integrated nanofluidic reactor enabled the digestion, separation, and UV detection of a 1 pL cytochrome c sample within a single device. The reaction rate was 24–48 times faster than that in the bulk system	b. 47
	c. w 1.2 mm × d 310 nm × L 50 mm	c. 3.2 × 10^6 m^{-1}	c. 16 min	c. 9.0 nL min^{-1}		c. Cytochrome C	c. Protein digestion was accelerated by 12–178-fold using thin-layer nanochannels combined with a numbering-up strategy, enabling product collection at the microliter scale.	c. 48
Glass capillary	Open tubular i.d. 10 μm × 30 cm	4.0×10^6 m^{-1}	0.5–2.5 min	30 nL min^{-1}	Trypsin	Cytochrome C, β-casein, Myoglobin, Melittin	An open tubular capillary enzyme reactor enables rapid atto–femtomole protein digestion with direct on-line integration into CE-ESI-MS for fast protein identification.	49
Glass	Nanochannel							
	a. w 3.3 μm × d 200 nm × L 130 μm	a. 5.0 × 10^6 m^{-1}	a. ~2 min	a. ~86 fL/2 min	a. Anti-mouse IgG (antibody)	a. DyLight488-labeled mouse IgG (antigen)	a. A nanofluidic immunoassay achieves near-100% capture efficiency in an 86 fL reaction space, enabling quantitative detection to 3 zmol.	a. 50
	b. w 2 μm × d 770 nm × L 3 mm	b. 1.3 × 10^6 m^{-1}	b. ~2 min	b. ~4.6 pL/2 min	b. IL-6 antibody	b. IL-6 (antigen) and HRP-conjugated anti-IL-6 polyclonal antibody	b. An integrated micro/nanofluidic platform enables ELISA-based detection of IL-6 secreted from living single B cells through hierarchical fL-pL processing.	b. 35
	Microchamber							

Table 1 *(Contd.)*

Material	Channel/reactor dimensions	Specific surface area	Reaction time	Productivity	Immobilized enzyme (or free enzyme)	Reaction sample (or substrate)	Highlight	Ref.
a. CYTOP-coated glass	a. Dia 5 μm × h 3 μm (bead size: 3 μm)	a. 6.3×10^5 m^{-1}	a. ~2 h	a. ~60 fL/2 h	a. Streptavidin-β-galactosidase	a. Prostate specific antigen (PSA) and monoclonal anti-PSA	a. A digital ELISA platform based on immobilized femtoliter droplets achieves ultrasensitive biomolecule detection with a LoD down to 2 aM by large-scale digital counting.	a. 51
b. Acrylic resin	b. Dia 3.5 μm × h 3.5 μm (magnetic beads size: 1 μm)	b. 9.5×10^4 m^{-1}	b. ~10 min	b. ~30 fL/10 min	b. Cas13a enzyme	b. SARS-CoV-2 RNA	b. Microchamber-based digital RNA detection combined with CRISPR–Cas13a enables amplification-free, rapid (<10 min) detection of SARS-CoV-2 genomic RNA.	b. 52
PDMS	Droplet (50–90 μm dia.)	—	~2.5 h	50, 75 μL min^{-1}	DNA polymerase	KRAS G12D mutant DNA Cancer-specific genome	Integrated droplet digital PCR assays combining microfluidic partitioning, multiplex PCR, and large-volume droplet counting enable 50–1000-fold higher sensitivity for detecting rare cancer-specific genomic targets.	53
CYTOP-coated glass	Microchamber dia. 4.3 μm, h 3 μm	—	40 min	~40 fL/40 min	Alkaline phosphatases, tyrosine phosphatases, and ectonucleotide pyrophosphatases	4-Methylumbelliferyl phosphate (model fluorescence substrate)	Microdevice-based multiplexed single-molecule assays enable ultrasensitive detection and subtype-resolved profiling of enzymatic activities in blood samples.	54

can proceed more rapidly compared with conventional bulk reactions. Prior work has shown that reactions occurring in a microchannel proceed at twice the rate relative to conventional bulk reactions.[57] Rapid enzymatic reactions have also been observed in nanochannels.[58] Based on their ability to provide efficient reactions with small sample volumes, micro and nanofluidic bioreactors have become promising research tools (Fig. 2(a)).

One of the most successful applications of bioreactors has been as polymerase chain reaction (PCR) devices. Using state-of-the-art microfluidics, rapid PCR can be achieved with increased flexibility.[60] PCR typically involves repeated thermal cycling to provide the temperatures required for denaturation, annealing and extension during each amplification cycle. Several different rapid PCR reactors have been developed over the past two decades.[61] The first continuous flow microfluidic PCR was fabricated by Kopp *et al.*[59] In this device, the reagent was introduced into a channel having distinct zones maintained at the different temperatures necessary for denaturing, annealing and extension (Fig. 2(b)).

In recent years, bioreactors have often been used as medical assay or biological analysis platforms, in contrast to the chemical reactors employed for large-scale continuous reactions.[56] As an example, a digital integrated droplet PCR assay was developed as a means of profiling circulating tumor DNA (Fig. 2(c)).[53] This device was integrated with microfluidic droplet partitioning, multiplex PCR amplification and large-volume droplet counting processes. The resulting assay was able to detect rare cancer-specific genomic targets and provided a sensitivity 50 or 1000 times greater than those associated with standard dPCR and qPCR assays, respectively. The incorporation of droplet or microwell structures has also allowed the construction of portable, automated PCR reactors for the rapid detection of viruses such as COVID-19 and for diagnostics.[52,62,63] Notably, single enzyme activity has been assessed based on confining enzymes and substrates in microwells (that is, the use of droplets).[54,64] The confinement of disease-related proteins in microwells has also allowed the enzymatic activity of individual molecules to be investigated (Fig. 2(d)). This method can be used to monitor fluctuations in enzyme activity or assess abnormal activity at the single enzyme level.[65] Bioreactors have thus been increasingly utilized as assay and biological analysis platforms.

The analysis of enzyme kinetics is a vital aspect of evaluating enzyme-catalyzed reactions in micro and nanoreactors. The enzyme/substrate concentration ratio, temperature, pH, solvent and flow rate (meaning flow pressure) all play important roles in such evaluations. Enzyme kinetics are typically analyzed using the Michaelis–Menten model. Studies to date have shown that enzymatic reactions in microchannels are accelerated by factors of 2 to 20 times compared with bulk reactions.[57,66,67] However, the mechanism by which this acceleration occurs remains unclear. This phenomenon can possibly be explained by the rapid mass transport, increased diffusion rates and enhanced mixing in microchannels as substrates come into contact with active sites. The greater reactiv-

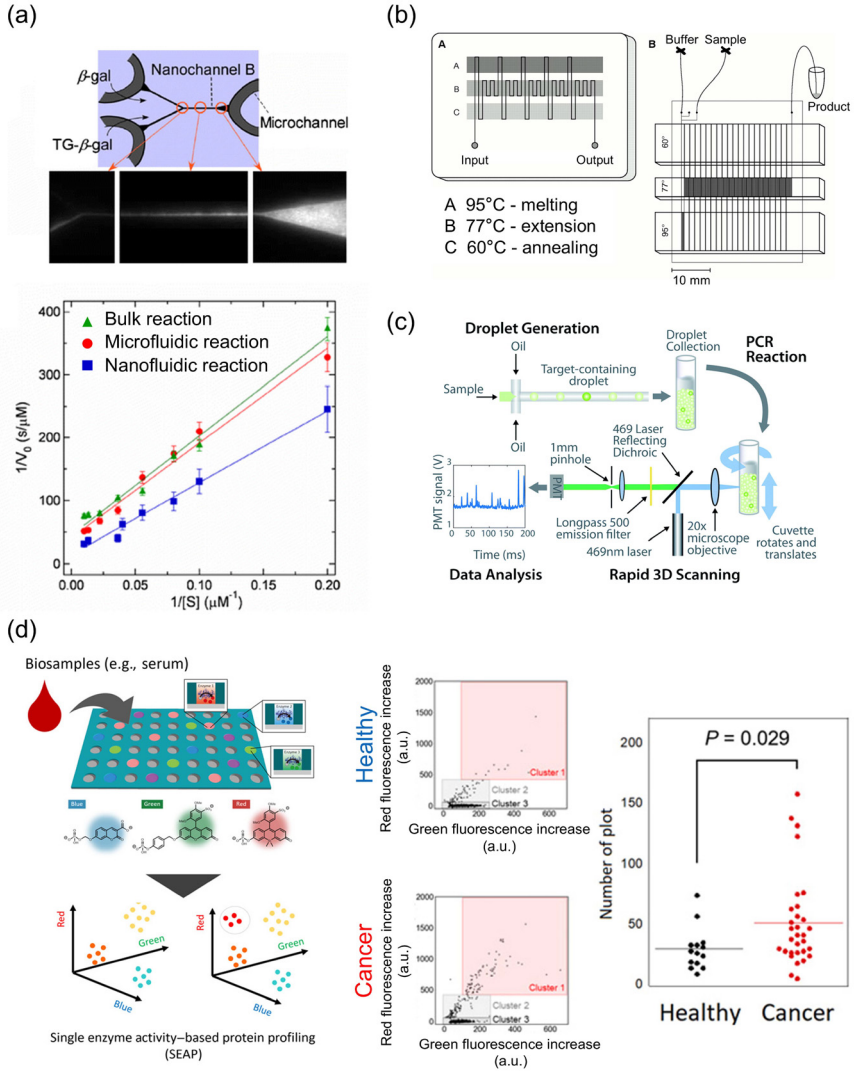

Fig. 2 Liquid phase bioreactors. (a) A diagram and photographic image of a continuous-flow enzyme reaction in a nanochannel (upper). A series of Lineweaver–Burk plots based on initial reaction rates, showing that the rate of the enzyme reaction in the nanofluidic reactor was twice that in the bulk (lower). Reprinted with permission from Springer.[58] © Springer Nature 2008. (b) Diagrams showing continuous-flow PCR on a microfluidic device with PCR amplification based on successive heating and cooling (Reproduced with permission from ref. 59). From M. U. Kopp, A. J. d. Mello, A. Manz, Chemical Amplification: Continuous-Flow PCR on a Chip, *Science*, 1998, **280**(5366), 1046–1048. Reprinted with permission from AAAS. (c) A diagram showing DNA profiling by digital droplet detection. The reaction platform shown allows the partitioning of pL-sized droplets with thermal cycling to amplify specific fluorescence signals. This system can also detect and quantify droplets that are positive for one or more specific target analytes. Reproduced from ref. 53 with permission from the Royal Society of Chemistry. Copyright 2019 The Royal Society of Chemistry. (d) A diagram of a microwell bioreactor for the analysis of single molecule enzyme activity. The reactivities toward differentially colored and structured substrates are used to characterize the enzyme species in each well. Enzyme activity can be profiled at the individual enzyme level, revealing differences in enzyme activity between healthy donors and cancer patients at the single-molecule scale (Reproduced with permission from ref. 54). From S. Sakamoto, T. Komatsu, R. Watanabe, Y. Zhang, T. Inoue, M. Kawaguchi, H. Nakagawa, T. Ueno, T. Okusa K. Honda H. Noji, Multiplexed single-molecule enzyme activity analysis for counting disease-related proteins in biological samples, *Science Advance*, 2020, **6**, eaay 0888. Reprinted with permission from AAAS.

ity in micro and nanochannels can also be explained by external factors. That is, kinetic parameters may be changed due to variations in the flow rates in the channels,[68,69] and the mechanisms involved with efficient reactions involving so-called free state enzymes have been investigated. The flow state in microchannels is typically laminar because, at least theoretically, the associated Reynolds number (Re) is very small. Under flow-through conditions, the value of K_m (Michaelis constant) also decreases as the flow rate in the channels is increased, indicating more efficient complex formation between the enzyme and substrate. Evidently, the enzymes are used more efficiently in these channels compared with the bulk reaction.

On going from the micro to nanoscale, both thermal conductivity and molecular diffusion are promoted while sample losses are reduced. However, rather than simply scaling down,

the different liquid properties that appear on the nanoscale may affect reaction activity. As an example, increased turnover values, k_{cat}, have been reported in nanospaces.[70] This enhancement can be explained by two factors. Firstly, nanochannels provide a confined environment for enzymes that mimics the crowded conditions in living systems. The confinement of an enzyme in a nanospace could increase the thermodynamic stability of the molecule, similar to the mechanism that stabilizes protein folds in a cell.[71] Thus, higher enzyme activity may be achieved. Secondly, a nanochannel can provide an ideal space for homogeneous enzyme reactions based on the increased diffusional mixing of biomolecules. Nanoconfinement increases the rates of enzyme reactions and accordingly provides larger k_{cat} values. In prior experiments, enzymatic reactions were accelerated in nanochannels with dimensions on the order of 100 nm[58] and the k_{cat} values obtained in these nanoreactors were found to be twice those in microreactors or under bulk conditions. Biomimetic nanochannels[72] have been demonstrated to greatly affect both K_m and V_{max} (maximum reaction rate value) depending on the channel size and shape. Reaction rates in nanochannels are evidently increased because the proton (H^+) exchange rate is increased approximately tenfold as a result of the specific properties of water under such conditions. It is thought that hydrolysis reactions are promoted by the abundant proton supply in such systems. Assuming that micro and nanoreactors may have differing characteristics, such as varying mass transport and mixing properties, this may lead to different kinetic laws. Therefore, in future it will be important to assess the mechanisms by which enzymatic reactions are accelerated in such systems.

2.2 Heterogeneous catalyst for biochemical reactors

Micro and nanofluidic reactors incorporate solid supports having high S/V ratios, and so immobilizing enzymes on these supports can lead to highly efficient enzymatic reactions.[73] Specifically, immobilized enzyme reactors operated in micro- and nanofluidic formats can achieve markedly shorter reaction times, ranging from minutes to seconds rather than many hours, together with increased sample throughput. These enhancements arise from improved mass transfer under flow conditions, including reduced diffusion distances, convective transport of substrates, and high local concentrations of immobilized enzymes. An immobilized enzyme reactor can provide advantages such as convenience in handling, ease of separation of enzymes from the reaction mixture, high stability and reuse.[74,75] These reactors can generally be categorized into three types[76] (Fig. 1(b)). The first of these is known as the packed bead column, in which the enzyme is immobilized on a support material made of particles or beads that can be homogeneously packed into the microfluidic system. Typically, this configuration provides S/V ratios on the order of 10^4–10^6 m^{-1}, and is widely used because the particle size (ranging from 100 nm to 100 μm) and material can be readily tailored. Recently, rather than developing new bead reactor architectures, disposable cartridge-type packed-bed reactors have been commercialized[77] and applied mainly in analytical fields such as proteomic analysis. The second type comprises the monolithic column, in which the enzyme is immobilized in a network of micro- and nanoscale pores (ranging from 100 nm to 100 μm) within a monolithic material. Such sponge-like structures are often fabricated *via* bottom-up approaches, and generally exhibit S/V ratios on the order of 10^4–10^6 m^{-1}. More recently, hydrogel-based supports with strong enzyme affinity and extremely high S/V ratios (on the order of 10^8 m^{-1}) have been increasingly reported.[45,78] However, when the pore size of the gel approaches ~10 nm, macromolecular substrates may no longer be able to penetrate the porous network, necessitating careful control of pore size to ensure accessibility of proteins and other large biomolecules (*e.g.*, polysaccharides, nucleic acids).[79] Finally, in a wall-coated column, the enzyme is directly attached to the inner surface of a flow path comprising a capillary or micro/nanochannel. Unlike packed-bed and monolithic reactors, this approach avoids porous structures; therefore, it is expected to mitigate reproducibility issues arising from sample carryover. In bead and monolith systems, the porous and structurally heterogeneous architecture can lead to unstable flow profiles and local stagnation, while molecular trapping within pores has also been reported, potentially causing significant carry over.[79] To overcome these limitations, wall-coated nanofluidic reactors with characteristic dimensions of 10–100 nm offer S/V ratios on the order of 10^6–10^7 m^{-1}. Furthermore, numbering-up of nanochannels is expected to enable both highly efficient reactions and improved productivity.

An immobilized enzyme reactor platform is a useful means of accelerating enzymatic reactions. The optimal design and configuration of an immobilized enzyme reactor are selected depending on the support material (such as natural polymers, glass or metals) and immobilization method (adsorption, covalent bonding, affinity interactions or entrapment).[76,80] Herein, the focus is on the optimal immobilization methods and latest applications for efficient biological reactions.

Immobilization methods providing the greatest efficiency and reusability have been studied. Typically, enzymatic activity is linked to the stability of the enzyme structure. However, there are several specific challenges associated with enzyme immobilization, related to controlling the enzyme density and orientation, the interactions between the enzyme and the support material, and adjusting pore size. A combination of enzyme and support material that undergoes strong interactions must be selected because enzymatic activity will vary depending on the affinity between the biomolecule and the support material.[79] In most cases, interactions between the enzyme and the support will lead to some enzyme distortion having negative effects on activity due to steric hindrance. These interactions may involve reactive groups on the support (such as multipoint covalent immobilization) or interactions with the matrix.[81] Secondly, the immobilized enzyme density must be optimized. At high densities, the apparent enzyme activity is generally increased, whereas excessive densities can decrease the activity as a result of steric hindrance.[82] As an

example, the digestive enzyme protease is known to exhibit self-digestion so that it is necessary to immobilize this compound on the surface at a specific density.[83] Thirdly, in the case that the immobilized enzyme is in the incorrect orientation, the substrate molecule is prevented from accessing active sites on the immobilized molecule as a consequence of pore size or steric limitations. This steric problem can be solved using protocols that enable specific enzyme orientations.[84] Specifically, a method of controlling orientation using affinity peptide tags has been devised[85] and has been used to control the orientation of biomolecules. In this process, the desired orientation is selected by screening for peptide sequences exhibiting high affinity for the solid support. In this manner, it becomes possible to orient the target moiety in a desired direction while avoiding undesired interactions between the target moiety and the solid surface. This technique has been shown to increase the activity of the immobilized enzyme by up to tenfold in specific systems.[85]

An additional steric issue arises when the substrate size exceeds the pore size of the support on which the enzyme is immobilized.[79] In this scenario, in which a large macromolecule (*e.g.*, large proteins, polysaccharides, nucleic acids) much larger than the enzyme is employed, the substrate is unable to access the immobilized enzyme in the porous space. It is important to provide well-defined spaces and regular immobilization patterns so that the substrate can diffuse freely in the small nanochannels. A method of directly immobilizing reactants in confined nanochannels has been developed[50] in which some silanol groups on the glass surface of the nanochannel are replaced with amino groups *via* silane coupling, after which the enzyme (an antibody) is grafted to these surfaces using a cross-linker. Although this is a standard technique for surface modification, it has proven useful as a means of achieving stable liquid flows and regulated immobilization in well-defined spaces. Such work has allowed micro and nanochannels to function as suitable reaction platforms while overcome diffusional limitations in narrow spaces. The following Sections (2.2.1–2.2.3) describe the structural characteristics, operating principles, and advantages of each reactor type. Subsequently, Sections 2.2.4 and 2.2.5 introduce representative applications of these reactors in proteomics and diagnostic assays, respectively.

2.2.1 Packed-bed microreactors. Packing microchannels or capillaries with functionalized particles are versatile tools for fabricating microreactors. In typical chip-based or capillary packed-bed systems, the reactor volume is on the order of 0.5–5 μL and the structured packing provides surface-to-volume ratios on the order of 10^3–10^4 cm^2 mL^{-1}, which enables high biocatalyst loads, enhances mass transport and significantly shorter reaction times. However, defining the optimal operating window requires a critical understanding of the interplay between convection and diffusion at varying flow rates. This characterization is often non-trivial; accurately simulating solute transport within packed-bed microreactors remains a challenge, and is particularly difficult in systems where the molecular diffusivity of the solute is very low.[86] This efficiency is demonstrated in applications such as rapid protein digestion, where complex proteins that normally require 2–16 h in solution can be digested within about 2–10 min at flow rates of roughly 0.5–5 μL min^{-1}, without sacrificing sequence coverage.[45,87] Other applications include enzymatic assays, inhibitor screening and immunotrapping, which similarly exploit high enzyme loadings in microliter-scale packed-beds.[88,89]

Two primary strategies are used to retain beads within the microreactor. The first is physical trapping, in which particles are contained by micromachined structures, including weirs or pillar-type filter arrays, that are often incorporated into silicon or polymer chips. However, scaling up these devices based on widening the channels can lead to non-uniform flow, necessitating the addition of flow distributors such as triangular prechambers to maintain performance and prevent channeling, especially in reactors with multiple particle layers.[86,90] The second strategy for capillary-based systems is the magnetic bead microreactor. In this setup, a small plug of enzyme-coated superparamagnetic particles (typically forming a bed volume of <1 μL inside a capillary of a few tens to a few hundreds of micrometers in diameter) is injected into the capillary and held in place by an external magnet.[88,89,91] This design is simple, automatable and allows the bead plug to be easily replaced after each run, eliminating the need for solid-phase regeneration. This platform has been extended to create advanced systems, such as dual-enzyme microreactors in which two distinct plugs of enzyme-coated beads are immobilized in series within a single capillary to perform sequential reactions or simultaneous multi-substrate analyses.[45,91]

One of the key challenges related to these systems is the need to achieve uniform flow distribution to prevent fluid channeling, which can otherwise reduce efficiency and catalyst accessibility.[86,90] Sample carryover is another concern, requiring robust washing protocols between analyses.[42,87] In the case of magnetic systems, the degree of reproducibility also depends on the consistent injection of a uniform bead suspension and ensuring that the quantity of beads does not overload the magnetic trap.[88]

2.2.2 Monolithic column microreactors. Monolithic microreactors feature rigid, continuous macroporous polymer supports prepared by *in situ* polymerization within capillary or microfluidic channels. A representative design is a 0.59 μL porous polymer monolith in a fused-silica capillary with a porosity of ~75%, corresponding to ~0.44 μL pore volume for convective flow and ~0.15 μL solid phase for enzyme anchoring.[92] This method creates a highly permeable structure that offers low back pressure, enabling high flow rates and rapid, convection-dominated mass transport that is not limited by diffusion.[93,94] Enzymes such as trypsin can be immobilized on the monolith *via* covalent interactions at loadings of the order of low- to mid-nmol per μL of monolith, providing extremely high local concentrations that suppress self-digestion and dramatically accelerate proteolysis. In such systems, protein digestion times can be reduced from hours to seconds or minutes; for example, myoglobin digestion in a chip-based monolithic

reactor at 0.5 μL min^{-1} (residence time ≈11.7 s) has yielded ~60–70% sequence coverage in a single pass.[92] As such, these reactors are well-suited to high-throughput, automated applications such as on-line peptide mapping when coupled with mass spectrometry[43,95] or capillary electrophoresis.[94] Photolithographic techniques can also enable the creation of integrated, dual-function devices that combine processes such as solid phase extraction and enzymatic digestion within a single unit.[44]

Despite the advantages of this technology, the performance that can be achieved is highly dependent on operational parameters. The flow rate, which dictates the substrate's residence time, is the most significant factor affecting the extent of digestion; systematic studies varying residence times from ~5 s up to several minutes show that higher flow improves mass transfer but eventually reduces the contact time needed for near-complete digestion.[93,96] Furthermore, the inherent hydrophobicity of some polymer monoliths can lead to the non-specific adsorption of proteins and peptides. This often necessitates the addition of organic solvents like methanol to the mobile phase, a modification that can also improve digestion efficiency.[95]

2.2.3 Wall-coated microfluidic reactors. Wall-coated microreactors, also known as open-tubular microreactors, are created by attaching enzymes to the inner surfaces of narrow-bore fused-silica capillaries or nanochannels. These devices offer significant advantages over homogeneous solution methods, including enhanced enzyme stability, reusability and the suppression of enzyme autolysis, which simplifies analysis.[49,97] A key aspect of these systems is the maximization of the S/V ratio based on using capillaries having small inner diameters of 10–50 μm, which drastically reduces substrate diffusion times to allow digestion in minutes or seconds.[98] For example, an i.d. 50 μm × 140 cm trypsin capillary operated at 1–5 μL min^{-1} provides residence times of ~30–160 s and can completely digest model proteins such as cytochrome c in <5 min total analysis time.[99] Various immobilization strategies are employed in conjunction with such devices, including covalent attachment *via* linkers such as glutaraldehyde,[97] highly specific non-covalent binding using the strong biotin–avidin interaction,[100] immobilization with genetically engineered tags such as the Zbasic2 module for oriented attachment[101,102] and electrostatic adsorption *via* renewable layer-by-layer assembly.[103] These reactors are widely used for rapid protein digestion and peptide mapping. They are also often coupled directly to separation techniques such as capillary electrophoresis and mass spectrometry for the automated analysis of minute sample volumes and can even function as electrospray needles.[49,104] These wall-coated reactors provide highly controlled reaction environments with minimal dead volume and excellent reproducibility. Based on these structural platforms, various micro- and nanofluidic enzyme reactors have been implemented in analytical and diagnostic applications, as discussed in Sections 2.2.4 and 2.2.5.

2.2.4 Applications in proteomics. In a typical proteomics procedure, proteins are digested to generate peptide fragment by a protease (generally trypsin) prior to analysis using liquid chromatography – mass spectrometry.[105] This process is performed in conjunction with a low enzyme concentration and a long incubation time (12–24 h) to prevent self-digestion of the free trypsin. However, the free trypsin in solution is unstable and so there is a gradual decrease in activity due to self-digestion. Over the last few decades, these issues have been addressed through the development of immobilized enzyme reactors allowing highly efficient proteolysis in conjunction with proteomics.[98]

Enzymes are often immobilized on the surfaces of monolithic or beaded support materials to increase the apparent enzyme concentration. In fact, these reactor types have become the most common immobilized enzyme systems.[80,106] However, the nonuniform spaces in such devices do not allow stable fluidic control, resulting in poor reproducibility and carry-over.[107] This problem becomes more significant when using large substrates such as polysaccharides, proteins and nucleic acids. In such cases, the active sites must be perfectly oriented towards the outside of the support surface for the immobilized enzyme to fully catalyze the substrate reaction. Even so, if the substrate is larger than the enzyme, the enzyme activity may be decreased whereas small substrates may be trapped within the pore, leading to carry-over.[79] Open channel enzyme reactors have been devised as a means of mitigating these concerns. In such systems, the enzyme is directly attached to the inner walls of a channel or capillary. This structure solves the problems of reproducibility and carry-over based on the regular construction of micro and nanoscale spaces.

Recently, it has become possible to perform advanced analyses such as single-cell proteomics owing to the miniaturization of reactions and well-defined spaces. Building on these advances, an ultra-fast pL-scale enzyme reaction system in which trypsin is immobilized on a nanochannel surface was developed.[46] This device was found to increase the enzyme reaction rate by a factor of 25 times compared with a conventional bulk method (Fig. 3(a)). A protein analysis device has been demonstrated that is integrated with an enzyme reactor to allow protein digestion, chromatography for peptide separation and UV detection in a single system (Fig. 3(b)).[47] This device enables rapid protein analysis together with multiple other processes on the fL-pL scale and can be used for the evaluation of extremely small volumes, such as in the case of single-cell analysis. It is evident that immobilized enzyme reactors based on nanofluidics have contributed to the development of systems involving novel protein digestion mechanisms and analyses based on extremely small volumes. These technological advances have not only expanded the applicability of immobilized enzyme reactors to nanoscale and single-cell analyses but have also prompted a deeper investigation into their underlying reaction mechanisms and kinetics. In addition, a recent nanochannel numbering-up technology was realized to increase the reaction volume in the nanochannels from pL-scale to nL-μL. As a result, the digested sample in the nanochannels was analyzed by conventional LC-MS, and 12–178

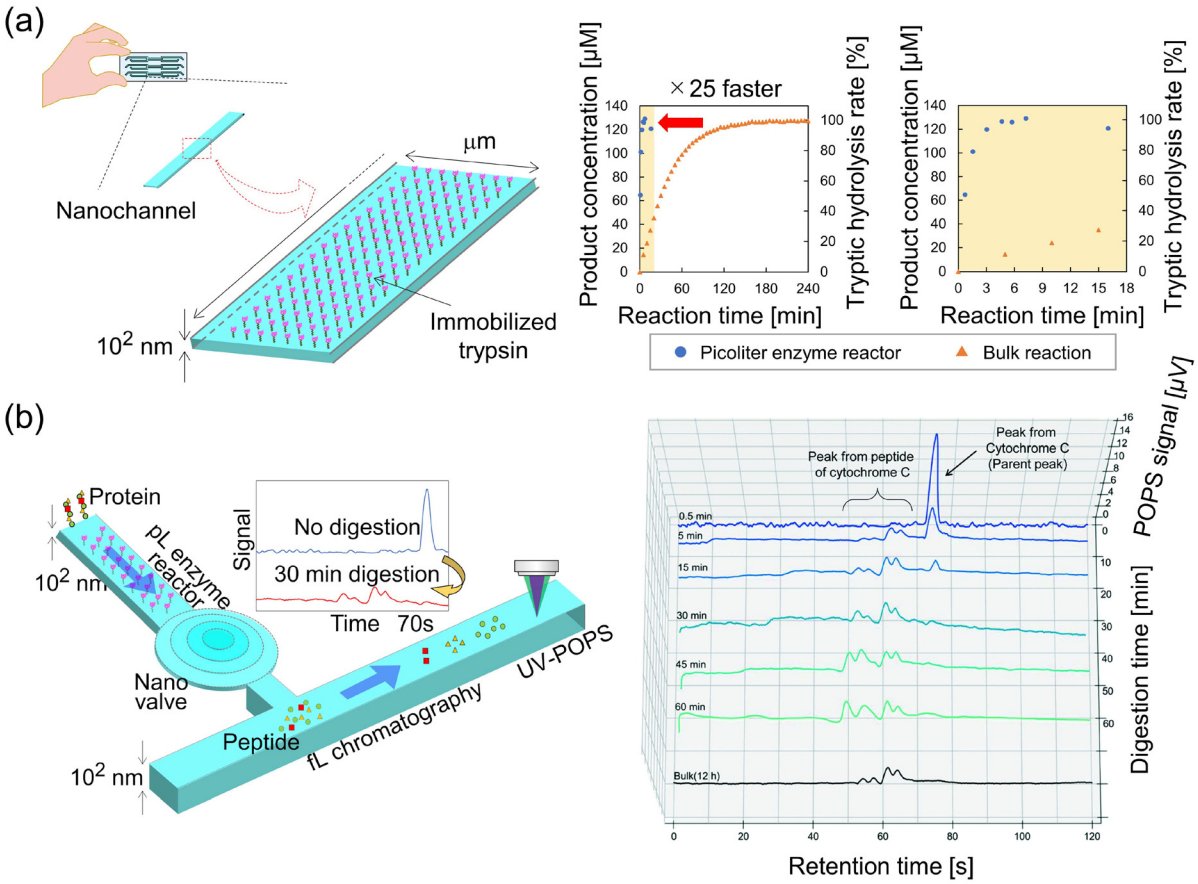

Fig. 3 Solid phase bioreactors for proteomic analysis. (a) A diagram showing the concept of an immobilized enzyme reactor in a nanofluidic device (left). Data indicating that the enzyme reactor accelerated the analysis by a factor of 25 times compared with the bulk reaction (right). Reproduced from ref. 46 with permission from the Royal Society of Chemistry. Copyright 2020 The Royal Society of Chemistry. (b) A concept for an integrated device for proteomic analysis involving pL to fL-scale channel volumes. The integrated device performs protein digestion, peptide separation and peptide detection in a volume of 1 pL within a single device (left). This device accelerated the enzyme reaction by a factor of 24–48 times compared with the bulk reaction (right). Reproduced from ref. 47 with permission from the Royal Society of Chemistry. Copyright 2022 The Royal Society of Chemistry.

times faster reaction was shown.[48] This technology enables more detailed analysis by conventional analytical instruments, and further clarification for reaction mechanism in the nanochannel can be expected.

Such reactors accelerate enzymatic reactions by increasing the apparent enzyme concentration.[108] However, quantitative evaluation of catalytic performance has been difficult due to nonuniform pore structures and unstable liquid transport. In other words, it can be challenging to determine the number of enzyme molecules per unit surface area if the spaces are nonuniform and the nanoporous material contains cracks. Moreover, it is difficult to accurately define reaction times because the liquid flow may not be stable. These issues have been addressed through the development of platforms allowing control over reaction volume, surface density and flow velocity.[83,109] Based on the fabrication of well-defined nanospaces combined with stable pressure-driven flow, such systems have been used to perform the first-ever investigations of the kinetics of immobilized enzymes in nanochannels. Using these devices, values for the Michaelis–Menten constant, K_m, maximum reaction velocity, V_{max}, and turnover rate, k_{cat}, have been experimentally determined. In such trials, the V_{max} value was found to be proportional to the apparent enzyme concentration in the immobilized enzyme reactor, whereas the K_m value decreased as the channel size was decreased. It should be noted that the evident decrease in K_m may have resulted from the effects of flow rate, enzyme immobilization and space size. The k_{cat} values associated with the immobilized enzyme were decreased compared with those for the free enzyme, although these values were approximately equivalent between immobilized enzyme reactors having different channel sizes. The decreases in k_{cat} may have resulted from various conformational changes as well as the effects of enzyme orientation and steric hindrance.[110] Data such as these have helped to elucidate the mechanisms by which immobilized enzyme reactors provide accelerated kinetics. Further kinetic analyses will deepen the understanding of reaction acceleration in immobilized enzyme reactors.

Alongside these kinetic advances, recent progress in miniaturization and ultrafast reactions has significantly improved proteomic workflows. However, achieving full protein coverage remains a major challenge. Parallel digestion with multiple proteases and improved separation or ionization performance are promising strategies to expand proteome coverage and enhance single-cell proteomics.[45] Furthermore, the integration of proteomics and multi-omics analyses will enable biological phenomena during development, regeneration, and aging at the single-cell level.[111]

2.2.5 Applications in diagnostic assays. Besides proteomics, immobilized enzyme platforms in micro- and nanofluidic formats have also been adapted to immunoassays. The enzyme-linked immunosorbent assay (ELISA) technique has been used for the quantification of various target molecules. In a typical ELISA method, an antibody is immobilized on the surface of a support material, after which a target antigen is captured and detected based on highly specific antibody–antigen interactions. Bioassays using this principle in conjunction with small reactor array systems have now become available. The most important benefit of bioassays in micro and nanoreactors is the ability to detect target molecules at extremely low concentrations. Historically, bead-based ELISA has been performed by packing microchannels with beads on which the antibodies are immobilized.[112] However, the channel sizes in such systems are limited by the bead diameter and so it has not been possible to continually reduce the reactor size. It is also difficult to achieve a stable liquid flow because air bubbles can be trapped in the packed beads[113] or carry over may occur.[114] It has been suggested that antibody-immobilized nanofluidic systems could mitigate these challenges. A micro or nanofluidic ELISA system would be able to integrate chemical processes such as mixing, separation and detection in parallel or in series, similar to an electric circuit. An ELISA device in which antibodies are partially immobilized on the nanochannel surfaces has been developed[50] and has demonstrated the capture of antigens for the immobilized antibodies with an efficiency close to 100%. As such, an extremely small amount of analyte can be captured in the nanochannel without sample loss, providing a high sensitivity five orders of magnitude greater than that achievable using a micro immunoassay. A single device for quantitative analysis was fabricated by integrating this ELISA methodology with other units.[115] This new system was then used for the analysis of a secreted cytokine (the target protein) produced by a single cell (Fig. 4(a)).[35] More recently, a novel ELISA device with switching valves has been reported as a means of implementing complicated fluidic manipulations.[116]

Although nanofluidic devices can be powerful tools for the analysis of ultra-small volumes including single cells or molecules, their direct application to clinical diagnostics remains challenging. For example, in the context of liquid biopsy samples such as saliva or urine, practical considerations become critical. These include the need to handle sufficiently large and manageable sample volumes, as well as the requirement to avoid clogging during assay operation. In this context, thin-layer ELISA has been proposed as an alternative strategy to enhance target capture efficiency. This concept relies on spatial confinement of analytes in the depth direction, which shortens diffusion distances and increases the collision frequency between target molecules and surface-immobilized capture antibodies, while also providing high effective surface-to-volume ratios. At the same time, clinically relevant sample volumes in the nL-μL range can be maintained (Fig. 4(b)).[117,118] Thin-layer reactors can have mm-scale widths and μm-scale depths and so provide high S/V ratios. These reaction systems have shown increased reaction efficiency in conjunction with nL volumes.

Digital bioassay systems represent a novel means of quantifying target molecules by combining an immobilized enzyme with microcompartments.[119] The main principle of such processes is the compartmentalization of the assay solution as a means of stochastically encapsulating individual target molecules within a reactor in a well or droplet, resulting in signal binarization with responses of "one" or "zero". Several previous studies have demonstrated highly sensitive detection based on encapsulating antibody-coated microbeads in wells or droplets. These methods have achieved sensitivities three to four orders of magnitude greater than those obtainable using conventional ELISA methods. Furthermore, single molecule studies using micro or nanofabrication technologies have enabled the preparation of well-defined fL or aL-scale reactors (Fig. 4(c)),[51] allowing single-molecule quantification and revealing enzyme heterogeneity that is obscured in ensemble measurements. Such developments are bridging the gap between analytical technology and fundamental molecular science, enabling direct observation of molecular behaviors at the single-enzyme level. Recent studies of single-molecule enzymatic reactions have revealed that individual enzymes can adopt multiple structural and functional states. With the advancement of AI-based structure prediction,[120–122] these findings have contributed to drug discovery and molecular diagnostics. However, although heterogeneity among single enzymes is becoming increasingly evident, its impact on overall biological function remains largely unexplored. In the future, miniaturized bioreactor technologies are expected to move beyond device engineering and serve as powerful tools for elucidating new aspects of molecular function.

3. Microfluidic and nanofluidic chemical reactors

3.1 Homogeneous catalysts for chemical reactors

Homogeneous catalysis using transition metal complexes has transformed synthetic chemistry by enabling highly selective reactions under mild conditions in solution. Classic examples include Wilkinson's $RhCl(PPh_3)_3$ catalyst, which can promote the rapid and stereospecific hydrogenation of alkenes, Grubbs' Ru-benzylidene (*N*-heterocyclic carbene) catalyst that mediates olefin metathesis across a broad substrate scope and Shvo's bifunctional diruthenium complex, which allows the hydro-

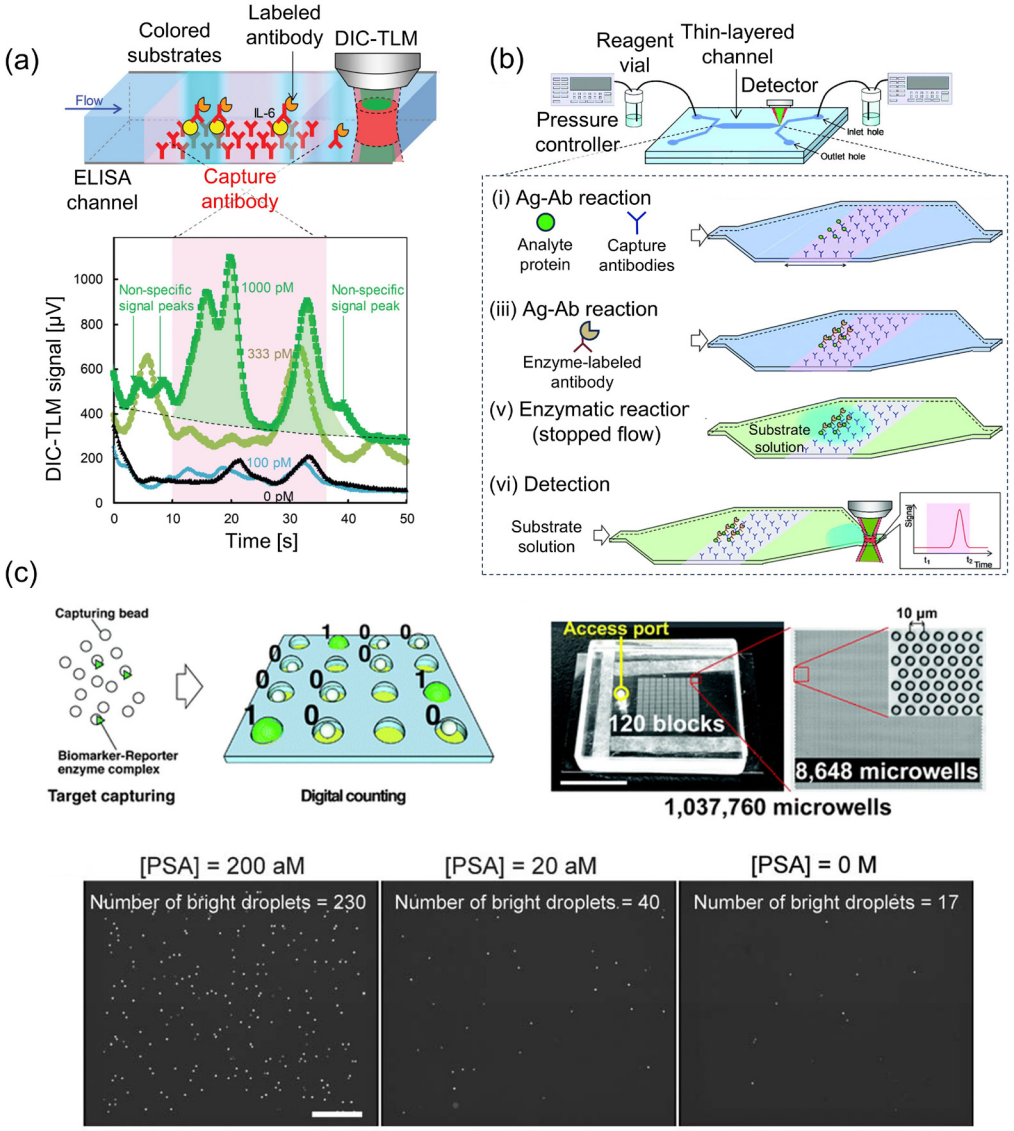

Fig. 4 A solid phase bioreactor for enzyme-linked immunosorbent assays. (a) A diagram of an integrated device for a secreted cytokine analysis. Reproduced from ref. 35 with permission from the Royal Society of Chemistry. Copyright 2019 The Royal Society of Chemistry. (b) Microfluidic ELISA utilizing a thin-layer channel, allowing the rapid analysis of target proteins with high sensitivity. Reproduced from ref. 117 with permission from the Royal Society of Chemistry. Copyright 2019 The Royal Society of Chemistry. (c) A microwell array device for the digital counting of single biomolecules. The scale bar in upper-right image is 1 cm. Digital signal counting was successfully demonstrated at attomolar concentration levels (0–200 aM range). The scale bar in the bottom image is 200 μm. Reproduced from ref. 51 with permission from the Royal Society of Chemistry. Copyright 2012 The Royal Society of Chemistry.

genation of carbonyl compounds without the use of an external H_2 source.[123–125] Iterations of these techniques that have tuned the electronic and steric environments, most notably through the use of chelating NHC ligands, have delivered turnover numbers exceeding 10^6 and enabled a high degree of control over *E*/*Z* selectivity (Table 2).[125]

However, the very solubility that confers a high level of activity on homogeneous catalysts also generates enormous practical challenges. Specifically, the separation of products from the catalyst is intrinsically difficult. Even state-of-the-art organic solvent nanofiltration and scavenger resins struggle to lower residual rhodium or palladium levels below the sub-ppm concentrations required by pharmaceutical regulations and the attendant losses of precious metals remain economically significant.[130,131] Air- and moisture-sensitive complexes also require the use of inert atmospheres, while ligand dissociation or metal center oxidation can shorten the catalyst lifetime and complicate scale-up.[132] Membrane-assisted recycling mitigates but rarely eliminates leaching, and so homogeneous catalysis is still largely confined to high-value, small-volume processes.[133]

On the basis of the above, the use of heterogeneous molecular catalyst systems within micro- or nanofluidic channels has become of interest. Immobilizing catalytic films, nano-

Table 2 Summary of typical chemical reactors

Type	Material	Channel/reactor dimension	Specific surface area	Reaction time/ conversion	Productivity/ Throughput	Product	Highlight	Ref.
Wall-coated	Pd immobilized on glass (microencapsulated)	w 200 μm d 100 μm L 45 cm	~1×10^4–5×10^4 m^{-1}	~2 min residence time	Hydrogen: 1000 μL min^{-1}; Substrate: 1.67 μL min^{-1}	Hydrogenated products (e.g., 4-phenyl-2-butanone)	Yield: 97% (1.4×10^5 times higher than conventional batch); No metal leaching detected; Quantitative yield in minutes	126
Packed-bed	Cartridge: stainless steel; Bead: activated carbon; Coated catalyst: Pd (10 wt% Pd/C)	Cartridge: i.d. 0.4 cm L 3 cm (30 mm CatCart®); Bead: 30–70 μm dia, 150 mg filled Frit: 8 μm pore size	~1.80×10^5 m^{-1}	< 1 min residence time: (flow 1000–2000 μL min^{-1});	Throughput: 1000–2000 μL min^{-1} (screening scale; ~60–120 g h^{-1} eq.)	Ethylbenzene (from Styrene reduction)	Conversion: 38–100% (variable); Automated screening; Identified cartridge variability and leaching issues	127
Magnetic particle	Fe_3O_4/SiO_2 amphiphilic nanospheres	Batch reactor (flask with stirring); Nanospheres <20 nm	~4.75×10^5 m^{-1}	~8 h (removal rate: 55%→96%)	~0.34 mmol product per run (90% conversion in 3 h)	Sulfones (*via* desulfurization of DBT)	Magnetic separation & recycling (3 cycles without loss); "Microreactor" refers to the particle itself	128
Monolith (CSM)	3D-printed Ti–6Al–4V/ stainless steel with Ni or Pt washcoat	Tubular reactor: i.d. 6 mm L 60 cm (4 × 15 cm units)	Geometric: ~10^3 m^{-1} (scaffold)	4.5–6.5 min residence time	Up to 55 g h^{-1} (flow: 3000 μL min^{-1})	Hydrogenated intermediates (e.g., from vinyl acetate)	Conversion: 90–100%; 3D printed geometry; low pressure drop; easy scale-up (tubular)	129

particles or packed-beds on channel walls can combined the extreme S/V ratios and short diffusion paths of microreactors with the ease of catalyst retention and reuse typical of solids, restoring near-homogeneous activities while simplifying downstream purification.[134,135]

3.2 Heterogeneous catalysts for chemical reactors

Heterogeneous catalysts used in the form of coatings[136] (Fig. 5(a) and (b)), packed/structured beds[137] (Fig. 5(c) and (d))

Fig. 5 (a) A schematic of a wall-coated catalyst microreactor. (b) A photographic image showing a $CuO/ZnO/Al_2O_3$ layer deposited on the internal wall of a 530 μm capillary. Adapted with permission from ref. 136. Copyright 2004, Elsevier. (c) A schematic of a packed-bed catalyst microreactor. (d) A photographic image of a glass tube with an inner diameter of 1.948 mm filled with copper particles having diameters of 80 μm (Adapted with permission from ref. 137. Copyright 2012, Elsevier). (e) A schematic of a batch reactor filled with catalyst-coated magnetic particles. (f) The oxidation of DBT to sulfone catalyzed by MSN/AEM–PTA particles (Adapted with permission from ref. 128. Copyright 2012, Elsevier).

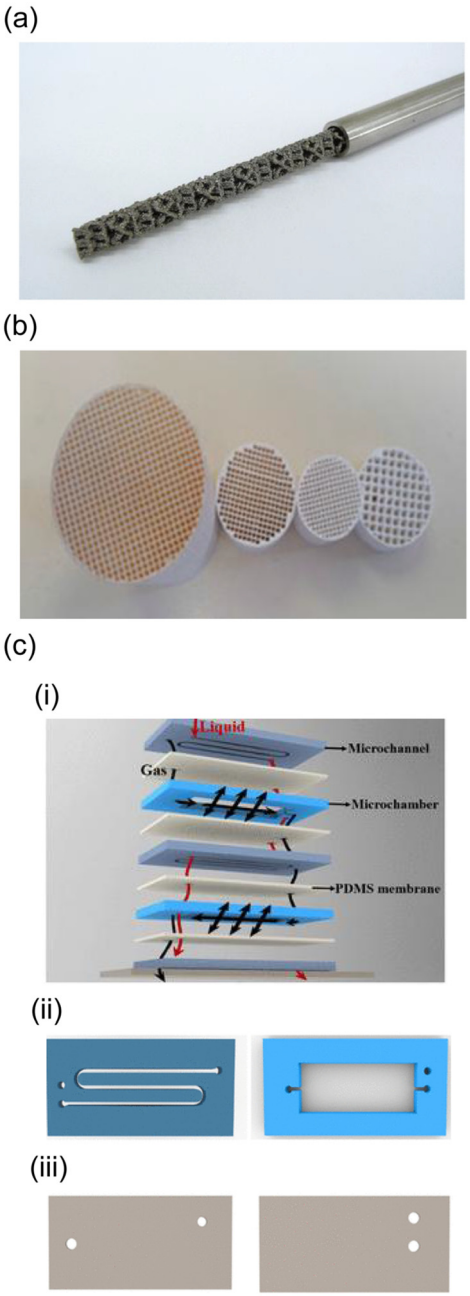

Fig. 6 Photographic images showing (a) a catalytic static mixer fitted inside a tube. Reproduced with permission from ref. 143, Copyright 2017, American Chemical Society. (b) Monoliths having different cell densities/sizes Reproduced from ref. 144, S. Govender *et al.*, *Catalysts*, 2017, **7**, 62, https://doi.org/10.3390/catal7020062, under CC BY 4.0. (c) Illustrations of (i) a stacked catalytic membrane microreactor, (ii) an independent perforated microchannel and microchamber and (iii) a PDMS membrane having two holes in different patterns Adapted with permission from ref. 138, Copyright 2020, American Chemical Society.

or membranes[138] (Fig. 6(c)) are frequently found in micro and milliscale reactors. In such devices, extreme S/V ratios, short diffusion paths and precise residence-time control can intensify reactions while allowing the active phase to remain fixed and recoverable. Rapid heat removal can also suppress the formation of hot spots and opens new process windows. Furthermore, lower transport resistance and narrow residence time distributions allow detailed analyses of kinetics. The minimal holdup associated with fixed catalysts allows the safe handling of hazardous gases such as H_2 and CO while also reducing work-up and catalyst losses and simplifying downstream separations. Finally, the use of modular hardware with inline analytics can accelerate design–make–test cycles.[135,139–142]

3.2.1 Wall-coated catalyst microchannel reactors. Immobilizing films of catalytic materials such as metals, oxides, zeolites and carbon directly on channel walls can permit near-plug-flow behavior at low pressure drops while providing diffusion lengths equal to approximately half the channel gap. These factors are advantageous when performing reaction rate studies under differential conversion conditions.[145–147] There are robust methods for the deposition of uniform zeolite/oxide coatings on metals, silicon or glass (including the deposition of single-layer ZSM-5 on stainless steel and the formation of sol–gel/washcoats with controlled porosities) and static-mixing inserts can be integrated to raise interfacial areas without using fine packings.[145–147] A representative demonstration is a Pd-immobilized glass microchannel reactor for gas–liquid–solid hydrogenation.[126] The device (200 μm × 100 μm × 45 cm channel) enabled quantitative hydrogenation and deprotection within 2 min under ambient conditions, leveraging exceptionally large gas–liquid–solid interfacial area and diffusion paths on the order of micrometers. No Pd leaching was detected by ICP, and space–time yields exceeded conventional batch reactors by over 10^5-fold, highlighting how wall-coated catalytic microchannels can realize both rapid kinetics and intrinsic cleanliness in continuous multiphase synthesis.[126] The use of photocatalytic films, typically comprising TiO_2, can generate micro-scale optical paths that suppress internal filtering. The resulting large interfacial areas can increase the quantum efficiency of volatile organic compound abatement and aqueous organics degradation processes under UV/visible light.[148,149] Recent microfluidic designs have allowed the quantification of photonic and hydrodynamic impacts on conversion, providing helpful guidance for scale-up and the development of light delivery strategies.[149]

3.2.2 Packed-bed catalyst microreactors. Packing short capillaries or cartridges (typically 0.5–3 mm i.d., yielding effective channel widths of 20–160 μm) with catalyst particles can concentrate the active surfaces and provide exceptional gas–liquid–solid mass transfer with minimal modest footprints. Hence, such systems have been applied to hydrogenation, hydrogenolysis and reductive amination reactions.[139,141,142] An example is the H-Cube® system, which allows on-demand H_2 generation *via* electrolysis and can be combined with CatCart® packed cartridges and controlled T, p, Q. This approach enables screening and small-scale synthesis within minutes under contained, cylinder-free conditions.[127,142] However, these systems are subject to critical failure modes that limit their robust operation. Uneven fluid

distribution can create zones of varying reaction rates and localized 'hot spots', particularly in exothermic hydrogenation reactions; these thermal gradients not only reduce selectivity and shorten catalyst lifespan but can also trigger reactor runaway. Furthermore, a fundamental trade-off exists between mass transfer and hydrodynamics: while reducing catalyst particle size enhances the interfacial area, it leads to significant pressure drops that restrict fluid flow and increase energy consumption. This limitation is exacerbated by high-viscosity solvents or complex multiphase flows, which further hinder gas–liquid mass transfer rates. Long-term operational stability is another challenge, as the formation of solid by-products (*e.g.*, coke or humins) can deposit on the catalyst, causing irreversible channel clogging. Finally, scaling up presents difficulties; increasing reactor diameter complicates thermal management due to radial temperature gradients, while parallelizing reactors risks inconsistent catalyst loading and flow maldistribution across channels.[150–152]

3.2.3 Magnetic particles as catalyst carriers: batch/on-chip actuation. Magnetic solids can enable catalyst retention and on-chip manipulation on small scales. In prior studies, amphiphilic Fe_3O_4@SiO_2 nanospheres bearing quaternary ammonium/phosphotungstic acid complexes have functioned as multifunctional microreactors for oxidative desulfurization[128] (Fig. 5(e) and (f)). Using these spheres, dibenzothiophene can be oxidized by H_2O_2 under mild conditions, after which the magnetic catalyst is simply retrieved and reused. This process has been found to reduce sulfur levels from 487 to <0.8 ppm under optimized conditions.[128]

Magnetic particles undergoing microfluidic flow can be trapped, transported, assembled into beds or deployed as mobile catalytic carriers. Some review summarizes the force landscapes, device concepts (such as magnetophoresis or on-chip capture/release) and early catalytic case studies, and explains the manner in which magnetic control promotes separation and overcomes mixing limits intrinsic to laminar microflows.[153] As an alternative to static trapping, time-dependent magnetic actuation allows control over the motion of catalytic particles. Experiments and modeling have shown that mass transfer coefficients depend on both the mean particle velocity and the variance in this velocity. An untuned periodic trajectory can decrease the mass transfer coefficient by up to 7.6% relative to the value associated with steady motion at the same mean speed. Such results highlight the need to optimize actuation protocols.[154]

3.2.4 Other types of heterogeneous catalytic microreactors. Catalytic static mixers[143] (Fig. 6(a)) are three dimensional printed or machined mixers whose surfaces are wash-coated with metals or oxides. These devices can deliver high k_L values and near-plug-flow at low pressure-drop values. There have been numerous demonstrations of the use of these systems in continuous hydrogenation reactions to produce fine chemicals and they have been found to remain durable throughout cleaning cycles, suggesting industrial applications.[129,143,155,156] However, the fabrication of these complex geometries *via* 3D printing remains cost-intensive, and the long-term stability of the washcoat layer under high-shear flow is a critical failure mode, where delamination can contaminate downstream processes.[157]

Structured/monolithic microreactors[144] (Fig. 6(b)) can be produced with honeycomb or foam units subjected to catalytic washcoats. These systems provide very low pressure drops at high flow rates while maintaining short film diffusion distances, although the two-phase distribution and coating adhesion must be carefully engineered.[144] A primary limitation of monoliths is their tendency towards laminar flow, which results in poor radial mixing compared to packed-beds; this can lead to broad residence time distributions (bypassing) unless segmented flow (Taylor flow) is strictly maintained.[158]

Catalytic membrane microreactors[138] (Fig. 6(c)) incorporate ceramic, zeolite, Pd alloy or polymeric membranes that combine reactions with selective permeation such as distributed H_2 dosing or *in situ* product removal. These devices can shift equilibria and improve selectivity. As an example, stacked micro-membrane designs have shown stable nitrobenzene hydrogenation with uniform gas delivery.[138,159] Nevertheless, these systems are prone to concentration polarization and membrane fouling (pore blocking), which can rapidly degrade flux rates. Furthermore, the mechanical fragility of ceramic membranes and the difficulty of reliable sealing at high temperatures pose significant hurdles for industrial scale-up.[160]

Metal organic framework (MOF)/zeolite hybrid membranes can be tailored to provide specific pore chemistries and, in some cases, concurrent separations. Prior works have studied Ag-loaded MOF microreactors for exothermic oxidations and the continuous-flow growth of ZSM-5 inside capillaries with controllable thickness and adhesion. Long-term mechanical/thermal stability remains the bottleneck to scaling up such systems.[161,162]

4. Conclusions and perspectives

This review summarized advances in catalytic reactions utilizing microfluidics/nanofluidics involving ultra-small spaces and short diffusion lengths. These channels provide rapid mixing and promote interactions between different phases. As such, improved performances with quick reactions, better yields and facile operation can be achieved. The development of new and unique reaction systems based on micro- or nanospaces is expected to have many benefits in the fields of chemistry and biochemistry. Moreover, as discussed, various unique reaction processes have been reported in such systems[58,72] as a consequence of the distinct properties of nanospaces. These unusual phenomena include higher conductivities,[163–167] greater proton mobility,[168,169] modified zeta potentials,[167,170,171] varied chemical equilibria[172] and lower dielectric constants.[171,173,174] These factors can possibly change reaction conditions and even the reaction mechanism such that certain reactions may only be realized in nanochannels. The need to increase the productivity of such systems remains challenging. Wall-coated micro or milliscale channel

reactors can provide relatively high productivity levels based on higher flow rates. Even so, such units exhibit lower S/V ratios compared with nanochannel devices and so show lower performance. Obtaining suitable S/V ratios together with high productivity levels could be possible using micro or milliscale channels packed with structures having nm-sized gaps. Such devices could permit μL or mL-scale flow rates. Despite this, the use of packing would lead to high operating pressures close to the MPa level as well as challenges in controlling the reaction conditions due to the unregulated gap sizes between the packed material. Especially, the concentration of the catalyst/enzyme in the nm-sized gap and the contact time of the liquid to the catalyst/enzyme on the surface in the nm-sized gap are still difficult to measure. Therefore, it is difficult to design the reactor with the packed material, and currently, reaction conditions are explored by trial and error. More advanced methods allowing the fabrication of uniform gaps and/or processes for the simulation of concentrations and reaction times are required. Another approach involves the numbering-up concept. In this case, size-regulated nanochannels could be fabricated as a means of improving performance. For example, reaction time is possible to control by controlling the flow rate of the nanochannels. The catalyst/enzyme concentration is possible to control by controlling the density and area of immobilized catalyst/enzyme and the volume of the liquid that contacts the catalyst/enzyme. These regulated and controlled nanospaces realize the design of the reactors by controlling reaction time, concentration, and temperature. Productivity can be enhanced by parallelizing nanochannels with dimensions comparable to, or smaller than, the nanopores found in bead- or monolith-based reactors. By increasing the number of such reactors, reaction throughput can be scaled up while maintaining regulated-nanoscale confinement. Unlike approaches based on packed structures, the numbering-up strategy preserves well-defined channel geometries, allowing nanoscale effects to be retained while increasing overall throughput. A remaining challenge lies in identifying approaches to improving productivity. This may involve new technologies for the numbering-up of nanochannels, especially along with improved fabrication methods for large areas and large numbers of nanochannels,[48,168,172] and nanofluidic control techniques to achieve uniform flow among the parallelized nanochannels.[18,48,175,176] These approaches allow us to move away from scale-down-based reactors, which have been developed through repeated trial and error without any established design. The numbering-up of size-regulated nanochannels will provide the basic design of the reaction (concentration, reaction time, temperature), the advantages of the nanochannel by extremely high S/V, and a breakthrough within the fields not only of analytical chemistry and bioanalytical chemistry, but also chemical and biochemical engineering.

Author contributions

B–Y. Z.: investigation, visualization, writing – original draft. K. Y.: investigation, visualization, writing – original draft. P-Y. C.: investigation, writing – original draft. K. M.: conceptualization, investigation, supervision, writing – original draft, writing – review & editing.

Conflicts of interest

There are no conflicts to declare.

Data availability

No primary research results, software or code have been included and no new data were generated or analysed as part of this review.

Acknowledgements

The authors gratefully acknowledge the financial support from the National Science and Technology Council, Taiwan (Grant No. NSTC113-2628-E-007-013-MY3).

References

1 D. R. Reyes, D. Iossifidis, P. A. Auroux and A. Manz, *Anal. Chem.*, 2002, **74**, 2623–2636.
2 P. A. Auroux, D. Iossifidis, D. R. Reyes and A. Manz, *Anal. Chem.*, 2002, **74**, 2637–2652.
3 G. M. Whitesides, *Nature*, 2006, **442**, 368–373.
4 P. Abgrall and N. T. Nguyen, *Anal. Chem.*, 2008, **80**, 2326–2341.
5 D. Mijatovic, J. C. T. Eijkel and A. van den Berg, *Lab Chip*, 2005, **5**, 492–500.
6 L. Bocquet and E. Charlaix, *Chem. Soc. Rev.*, 2010, **39**, 1073–1095.
7 H. Hu, Y. Zhuo, M. E. Oruc, B. T. Cunningham and W. P. King, *Nanotechnology*, 2014, **25**, 455301.
8 R. Peng and D. Li, *Nanoscale*, 2016, **8**, 12237–12246.
9 J. Li and D. Li, *J. Colloid Interface Sci.*, 2021, **596**, 54–63.
10 L. Sun, Z. Yin, L. Qi, D. Wu and H. Zou, *Microfluid. Nanofluid.*, 2016, **20**, 57.
11 L. Sun, L. Liu, L. Qi, R. Guo, K. Li, Z. Yin, D. Wu, J. Zhou and H. Zou, *Microsyst. Technol.*, 2020, **26**, 861–866.
12 L. H. Thamdrup, A. Klukowska and A. Kristensen, *Nanotechnology*, 2008, **19**, 125301.
13 E. Cheng, Z. Yin, H. Zou and L. Chen, *Microfluid. Nanofluid.*, 2015, **18**, 527–535.
14 E. Cheng, Z. Yin, H. Zou and P. Jurčíček, *J. Micromech. Microeng.*, 2014, **24**, 015004.
15 Z. Yin, E. Cheng, H. Zou, L. Chen and S. Xu, *Biomicrofluidics*, 2014, **8**, 066503.
16 L. Menard, J. Zhou, M. Woodson, C. Mair, J. Alarie and J. Ramsey, *Microsc. Microanal.*, 2012, **18**, 606–607.
17 D. G. Haywood, Z. D. Harms and S. C. Jacobson, *Anal. Chem.*, 2014, **86**, 11174–11180.

18 K. Morikawa, Y. Kazoe, Y. Takagi, Y. Tsuyama, Y. Pihosh, T. Tsukahara and T. Kitamori, *Micromachines*, 2020, **11**, 995.
19 Y. Tsuyama, K. Morikawa and K. Mawatari, *Nanoscale*, 2021, **13**, 8855–8863.
20 H. Kamai and Y. Xu, *Micromachines*, 2021, **12**, 775.
21 K. Morikawa, P. Chen, H. L. Tran, Y. Kazoe, C. Chen and T. Kitamori, *J. Micromech. Microeng.*, 2023, **33**, 047001.
22 H.-Y. Lee, P.-Y. Chen, W.-J. Soong, C. Chen and K. Morikawa, *J. Micromech. Microeng.*, 2025, **35**, 075014.
23 Y. Kikutani, A. Hibara, K. Uchiyama, H. Hisamoto, M. Tokeshi and T. Kitamori, *Lab Chip*, 2002, **2**, 193–196.
24 J. Hwang, Y. H. Cho, M. S. Park and B. H. Kim, *Int. J. Precis. Eng. Manuf.*, 2019, **20**, 479–495.
25 W.-J. Soong, C. Chen and K. Morikawa, *Biomicrofluidics*, 2025, **19**, 054102.
26 J. Atencia and D. J. Beebe, *Nature*, 2005, **437**, 648–655.
27 S. Raghu, *Exp. Fluids*, 2013, **54**, 1455.
28 C. Cavaniol, W. Cesar, S. Descroix and J. L. Viovy, *Lab Chip*, 2022, **22**, 3603–3617.
29 A. Mudugamuwa, U. Roshan, S. Hettiarachchi, H. Cha, H. Musharaf, X. Kang, Q. T. Trinh, H. M. Xia, N. T. Nguyen and J. Zhang, *Small*, 2024, **20**, 2404685.
30 A. A. Dos-Reis-Delgado, A. Carmona-Dominguez, G. Sosa-Avalos, I. H. Jimenez-Saaib, K. E. Villegas-Cantu, R. C. Gallo-Villanueva and V. H. Perez-Gonzalez, *Electrophoresis*, 2023, **44**, 268–297.
31 V. Miralles, A. Huerre, F. Malloggi and M. C. Jullien, *Diagnostics*, 2013, **3**, 33–67.
32 D. Erickson and D. Li, *Anal. Chim. Acta*, 2004, **507**, 11–26.
33 Y. Cong, Y. Liang, K. Motamedchaboki, R. Huguet, T. Truong, R. Zhao, Y. Shen, D. Lopez-Ferrer, Y. Zhu and R. T. Kelly, *Anal. Chem.*, 2020, **92**, 2665–2671.
34 Z. Y. Li, M. Huang, X. K. Wang, Y. Zhu, J. S. Li, C. C. L. Wong and Q. Fang, *Anal. Chem.*, 2018, **90**, 5430–5438.
35 T. Nakao, Y. Kazoe, E. Mori, K. Morikawa, T. Fukasawa, A. Yoshizaki and T. Kitamori, *Analyst*, 2019, **144**, 7200–7208.
36 M. P. Marques and N. Szita, *Curr. Opin. Chem. Eng.*, 2017, **18**, 61–68.
37 P. Ho, C. Westerwalbesloh, E. Kaganovitch, A. Grünberger, P. Neubauer, D. Kohlheyer and E. von Lieres, *Microorganisms*, 2019, **7**, 105.
38 Y. R. Maghraby, R. M. El-Shabasy, A. H. Ibrahim and H. M. E.-S. Azzazy, *ACS Omega*, 2023, **8**, 5184–5196.
39 K. Yamamoto, N. Ota and Y. Tanaka, *Anal. Chem.*, 2021, **93**, 332–349.
40 T. Sokač Cvetnić, A. Šalić, M. Benković, T. Jurina, D. Valinger, J. Gajdoš Kljusurić, B. Zelić and A. Jurinjak Tušek, *Catalysts*, 2023, **13**, 708.
41 A. Basso and S. Serban, *Mol. Catal.*, 2019, **479**, 110607.
42 H. Salim, R. Pero-Gascon, E. Giménez and F. Benavente, *Anal. Chem.*, 2022, **94**, 6948–6956.
43 D. S. Peterson, T. Rohr, F. Svec and J. M. J. Fréchet, *Anal. Chem.*, 2002, **74**, 4081–4088.
44 D. S. Peterson, T. Rohr, F. Svec and J. M. J. Fréchet, *Anal. Chem.*, 2003, **75**, 5328–5335.
45 F. F. Yuan, P. Wang, X. J. Han, T. T. Qin, X. Lu and H. J. Bai, *Sci. Rep.*, 2024, **14**, 15667.
46 K. Yamamoto, K. Morikawa, H. Imanaka, K. Imamura and T. Kitamori, *Analyst*, 2020, **145**, 5801–5807.
47 K. Yamamoto, K. Morikawa, H. Shimizu, H. Sano, Y. Kazoe and T. Kitamori, *Lab Chip*, 2022, **22**, 1162–1170.
48 F.-Y. Huang, P.-Y. Chen, P.-Y. Chen, C. Chen and K. Morikawa, *Anal. Sci.*, 2026, DOI: 10.1007/s44211-025-00867-w.
49 J. Křenková, K. Klepárník and F. Foret, *J. Chromatogr. A*, 2007, **1159**, 110–118.
50 K. Shirai, K. Mawatari and T. Kitamori, *Small*, 2014, **10**, 1514–1522.
51 S. H. Kim, S. Iwai, S. Araki, S. Sakakihara, R. Iino and H. Noji, *Lab Chip*, 2012, **12**, 4986–4991.
52 H. Shinoda, T. Iida, A. Makino, M. Yoshimura, J. Ishikawa, J. Ando, K. Murai, K. Sugiyama, Y. Muramoto, M. Nakano, K. Kiga, L. Cui, O. Nureki, H. Takeuchi, T. Noda, H. Nishimasu and R. Watanabe, *Commun. Biol.*, 2022, **5**, 473.
53 C. Y. Ou, T. Vu, J. T. Grunwald, M. Toledano, J. Zimak, M. Toosky, B. Shen, J. A. Zell, E. Gratton, T. J. Abram and W. Zhao, *Lab Chip*, 2019, **19**, 993–1005.
54 S. Sakamoto, T. Komatsu, R. Watanabe, Y. Zhang, T. Inoue, M. Kawaguchi, H. Nakagawa, T. Ueno, T. Okusaka, K. Honda, H. Noji and Y. Urano, *Sci. Adv.*, 2020, **6**, eaay0888.
55 P. Žnidaršič-Plazl, *Acta Chim. Slov.*, 2021, **68**, 1–16.
56 S. F. Berlanda, M. Breitfeld, C. L. Dietsche and P. S. Dittrich, *Anal. Chem.*, 2021, **93**, 311–331.
57 Y. Tanaka, M. N. Slyadnev, K. Sato, M. Tokeshi, H. B. Kim and T. Kitamori, *Anal. Sci.*, 2001, **17**, 809–810.
58 T. Tsukahara, K. Mawatari, A. Hibara and T. Kitamori, *Anal. Bioanal. Chem.*, 2008, **391**, 2745–2752.
59 M. U. Kopp, A. J. De Mello and A. Manz, *Science*, 1998, **280**, 1046–1048.
60 L. Gorgannezhad, H. Stratton and N. T. Nguyen, *Micromachines*, 2019, **10**, 408.
61 C. D. Ahrberg, A. Manz and B. G. Chung, *Lab Chip*, 2016, **16**, 3866–3884.
62 Z. Lin, Z. Zou, Z. Pu, M. Wu and Y. Zhang, *Acta Pharm. Sin. B*, 2023, **13**, 2877–2896.
63 T. Iida, J. Ando, M. Yoshimura, A. Makino, M. Nakano, Y. Kogo, H. Shinoda, M. Toyoda, T. Noda and R. Watanabe, *iScience*, 2024, **27**, 110868.
64 J. Ando, K. Murai, T. Michiyuki, I. Takahashi, T. Iida, Y. Kogo, M. Toyoda, Y. Saito, S. Murayama, M. Kurihara and R. Watanabe, *Proc. Natl. Acad. Sci. U. S. A.*, 2025, **122**, e2510559122.
65 P. Mogalisetti and D. R. Walt, *Methods Enzymol.*, 2016, **581**, 541–560.
66 A. J. Tušek, M. Tišma, V. Bregović, A. Ptičar, Ž. Kurtanjek and B. Zelić, *Biotechnol. Bioprocess Eng.*, 2013, **18**, 686–696.

67 M. Miyazaki, H. Nakamura and H. Maeda, *Chem. Lett.*, 2001, **30**, 442–443.
68 K. Yamashita, M. Miyazaki, H. Nakamura and H. Maeda, *J. Phys. Chem. A*, 2009, **113**, 165–169.
69 K. Yamashita, M. Miyazaki, Y. Yamaguchi, H. Nakamura and H. Maeda, *Lab Chip*, 2008, **8**, 1171–1177.
70 C. Wang, D. K. Ye, Y. Y. Wang, T. Lu and X. H. Xia, *Lab Chip*, 2013, **13**, 1546–1553.
71 D. Bolis, A. S. Politou, G. Kelly, A. Pastore and P. A. Temussi, *J. Mol. Biol.*, 2004, **336**, 203–212.
72 T. Saruko, K. Morikawa, T. Kitamori and K. Mawatari, *Biomicrofluidics*, 2022, **16**, 44109.
73 Z. Yao, Y. Li and W. Xu, *Analyst*, 2025, **150**, 3000–3010.
74 B. Wouters, S. A. Currivan, N. Abdulhussain, T. Hankemeier and P. J. Schoenmakers, *TrAC, Trends Anal. Chem.*, 2021, **144**, 116419.
75 Y. Asanomi, H. Yamaguchi, M. Miyazaki and H. Maeda, *Molecules*, 2011, **16**, 6041–6059.
76 Y. Zhu, Q. Chen, L. Shao, Y. Jia and X. Zhang, *React. Chem. Eng.*, 2020, **5**, 9–32.
77 I. Grunert, K. Heinrich, M. Hingar, J. Ernst, M. Winter, K. Bomans, K. Wagner, A. Fevre, D. Reusch, M. Wuhrer and P. Bulau, *J. Am. Soc. Mass Spectrom.*, 2022, **33**, 2319–2327.
78 M. Arad, C. Frey, R. Balagtas, R. Hare, K. Ku, D. Jereb, Z. Nestman, A. Sidhu, Y. Shi, O. Fordwour, K. M. Moon, L. J. Foster and G. Ghafourifar, *Anal. Chem.*, 2024, **96**, 18880–18889.
79 J. M. Bolivar, J. M. Woodley and R. Fernandez-Lafuente, *Chem. Soc. Rev.*, 2022, **51**, 6251–6290.
80 J. Zdarta, A. S. Meyer, T. Jesionowski and M. Pinelo, *Catalysts*, 2018, **8**, 92.
81 R. C. Rodrigues, C. Ortiz, Á. Berenguer-Murcia, R. Torres and R. Fernández-Lafuente, *Chem. Soc. Rev.*, 2013, **42**, 6290–6307.
82 B. Saha, J. Saikia and G. Das, *Analyst*, 2015, **140**, 532–542.
83 K. Yamamoto, K. Morikawa, C. Chen and T. Kitamori, *Anal. Sci.*, 2023, **39**, 251–255.
84 C. Garcia-Galan, Á. Berenguer-Murcia, R. Fernandez-Lafuente and R. C. Rodrigues, *Adv. Synth. Catal.*, 2011, **353**, 2885–2904.
85 Y. Kumada, Y. Tokunaga, H. Imanaka, K. Imamura, T. Sakiyama, S. Katoh and K. Nakanishi, *Biotechnol. Prog.*, 2006, **22**, 401–405.
86 F. Strniša, M. Bajić, P. Panjan, I. Plazl, A. M. Sesay and P. Žnidaršič-Plazl, *Chem. Eng. J.*, 2018, **350**, 541–550.
87 C. Wang, R. Oleschuk, F. Ouchen, J. Li, P. Thibault and D. J. Harrison, *Rapid Commun. Mass Spectrom.*, 2000, **14**, 1377–1383.
88 L. G. Rashkovetsky, Y. V. Lyubarskaya, F. Foret, D. E. Hughes and B. L. Karger, *J. Chromatogr. A*, 1997, **781**, 197–204.
89 X. Yan and S. D. Gilman, *Electrophoresis*, 2010, **31**, 346–352.
90 M. Bajić, I. Plazl, R. Stloukal and P. Žnidaršič-Plazl, *Process Biochem.*, 2017, **52**, 63–72.
91 J. Shi, W. Zhao, Y. Chen, L. Guo and L. Yang, *Electrophoresis*, 2012, **33**, 2145–2151.
92 S. Feng, M. Ye, X. Jiang, W. Jin and H. Zou, *J. Proteome Res.*, 2006, **5**, 422–428.
93 E. Calleri, C. Temporini, E. Perani, C. Stella, S. Rudaz, D. Lubda, G. Mellerio, J. L. Veuthey, G. Caccialanza and G. Massolini, *J. Chromatogr. A*, 2004, **1045**, 99–109.
94 M. Ye, S. Hu, R. M. Schoenherr and N. J. Dovichi, *Electrophoresis*, 2004, **25**, 1319–1326.
95 J. Křenková, Z. Bilková and F. Foret, *J. Sep. Sci.*, 2005, **28**, 1675–1684.
96 J. Duan, Z. Liang, C. Yang, J. Zhang, L. Zhang, W. Zhang and Y. Zhang, *Proteomics*, 2006, **6**, 412–419.
97 G. Ghafourifar, A. Fleitz and K. C. Waldron, *Electrophoresis*, 2013, **34**, 1804–1811.
98 H. Yamaguchi and M. Miyazaki, *Proteomics*, 2013, **13**, 457–466.
99 E. C. A. Stigter, G. J. De Jong and W. P. Van Bennekom, *Anal. Bioanal. Chem.*, 2007, **389**, 1967–1977.
100 L. N. Amankwa and W. G. Kuhr, *Anal. Chem.*, 1992, **64**, 1610–1613.
101 N. Miložič, M. Lubej, M. Lakner, P. Žnidaršič-Plazl and I. Plazl, *Chem. Eng. J.*, 2017, **313**, 374–381.
102 N. Miložič, G. Stojkovič, A. Vogel, D. Bouwes and P. Žnidaršič-Plazl, *N. Biotechnol.*, 2018, **47**, 18–24.
103 Z. Tang, T. Wang and J. Kang, *Electrophoresis*, 2007, **28**, 2981–2987.
104 L. Licklider, W. G. Kuhr, M. P. Lacey, T. Keough, M. P. Purdon and R. Takigiku, *Anal. Chem.*, 1995, **67**, 4170–4177.
105 R. M. Miller and L. M. Smith, *Analyst*, 2022, **148**, 475–486.
106 S. Datta, L. R. Christena and Y. R. S. Rajaram, *3 Biotech*, 2013, **3**, 1–9.
107 O. K. Brandtzaeg, B. T. Røen, S. Enger, E. Lundanes and S. R. Wilson, *Anal. Chem.*, 2017, **89**, 8667–8673.
108 E. G. Vlakh and T. B. Tennikova, *J. Sep. Sci.*, 2013, **36**, 1149–1167.
109 K. Yamamoto, K. Morikawa, H. Imanaka, K. Imamura and T. Kitamori, *Anal. Chem.*, 2022, **94**, 15686–15694.
110 J. M. Guisan, G. Fernandez-Lorente, J. Rocha-Martin and D. Moreno-Gamero, *Curr. Opin. Green Sustainable Chem.*, 2022, 100593.
111 X. Wang, M. Duan, J. Li, A. Ma, G. Xin, D. Xu, Z. Li, B. Liu and Q. Ma, *Nat. Commun.*, 2024, **15**, 338.
112 K. Sato, M. Tokeshi, T. Odake, H. Kimura, T. Ooi, M. Nakao and T. Kitamori, *Anal. Chem.*, 2000, **72**, 1144–1147.
113 K. Sato, M. Yamanaka, T. Hagino, M. Tokeshi, H. Kimura and T. Kitamori, *Lab Chip*, 2004, **4**, 570–575.
114 G. Ruan, M. Wei, Z. Chen, R. Su, F. Du and Y. Zheng, *J. Chromatogr. B: Anal. Technol. Biomed. Life Sci.*, 2014, **967**, 13–20.
115 K. Shirai, K. Mawatari, R. Ohta, H. Shimizu and T. Kitamori, *Analyst*, 2018, **143**, 943–948.
116 H. Sano, Y. Kazoe, R. Ohta, H. Shimizu, K. Morikawa and T. Kitamori, *Lab Chip*, 2023, **23**, 727–736.

117 T. Nakao, K. Mawatari, Y. Kazoe, E. Mori, H. Shimizu and T. Kitamori, *Analyst*, 2019, **144**, 6625–6634.
118 A. Smirnova, R. Ohta, E. Mori, H. Shimizu, K. Morikawa and T. Kitamori, *Anal. Methods*, 2023, **15**, 675–684.
119 H. Noji, Y. Minagawa and H. Ueno, *Lab Chip*, 2022, **22**, 3092–3109.
120 D. A. Silva, S. Yu, U. Y. Ulge, J. B. Spangler, K. M. Jude, C. Labão-Almeida, L. R. Ali, A. Quijano-Rubio, M. Ruterbusch, I. Leung, T. Biary, S. J. Crowley, E. Marcos, C. D. Walkey, B. D. Weitzner, F. Pardo-Avila, J. Castellanos, L. Carter, L. Stewart, S. R. Riddell, M. Pepper, G. J. L. Bernardes, M. Dougan, K. C. Garcia and D. Baker, *Nature*, 2019, **565**, 186–191.
121 S. Park, W. Jeong, Y. Kim, C. H. Lee and C. Seok, *Curr. Opin. Struct. Biol.*, 2025, **94**, 103084.
122 N. R. Bennett, J. L. Watson, R. J. Ragotte, A. J. Borst, D. L. See, C. Weidle, R. Biswas, E. L. Shrock, P. J. Y. Leung, B. Huang, I. Goreshnik, R. Ault, K. D. Carr, B. Singer, C. Criswell, D. Vafeados, M. G. Sanchez, H. M. Kim, S. V. Torres, S. Chan and D. Baker, *Nature*, 2026, **649**, 183–193.
123 C. O'Connor and G. Wilkinson, *J. Chem. Soc. A*, 1968, 2665–2671.
124 N. Menashe and Y. Shvo, *Organometallics*, 1991, **10**, 3885–3891.
125 S. B. T. Nguyen, R. H. Grubbs and J. W. Ziller, *J. Am. Chem. Soc.*, 1993, **115**, 9858–9859.
126 J. Kobayashi, Y. Mori, K. Okamoto, R. Akiyama, M. Ueno, T. Kitamori and S. Kobayashi, *Science*, 2004, **304**, 1305–1308.
127 M. C. Bryan, D. Wernick, C. D. Hein, J. V. Petersen, J. W. Eschelbach and E. M. Doherty, *Beilstein J. Org. Chem.*, 2011, **7**, 1141–1149.
128 X. Cui, D. Yao, H. Li, J. Yang and D. Hu, *J. Hazard. Mater.*, 2012, **205–206**, 17–23.
129 A. Avril, C. H. Hornung, A. Urban, D. Fraser, M. Horne, J. P. Veder, J. Tsanaktsidis, T. Rodopoulos, C. Henry and D. R. Gunasegaram, *React. Chem. Eng.*, 2017, **2**, 180–188.
130 H. Xiao, W. R. F. Goundry, R. Griffiths, Y. Feng and S. Karlsson, *Green Chem.*, 2025, **27**, 3186–3196.
131 M. Economidou, N. Mistry, K. M. P. Wheelhouse and D. M. Lindsay, *Org. Process Res. Dev.*, 2023, **27**, 1585–1615.
132 B. Lunelli and M. Baroncini, *Chem.: Methods*, 2021, **1**, 421–426.
133 M. Janssen, C. Müller and D. Vogt, *Green Chem.*, 2011, **13**, 2247–2257.
134 X. Chen, M. Fu, J. He, J. Lu, C. Wang, D. Jiang, Y. Li and C. Yu, *Coord. Chem. Rev.*, 2025, **538**, 216723.
135 A. Tanimu, S. Jaenicke and K. Alhooshani, *Chem. Eng. J.*, 2017, **327**, 792–821.
136 J. Bravo, A. Karim, T. Conant, G. P. Lopez and A. Datye, *Chem. Eng. J.*, 2004, **101**, 113–121.
137 B. Tidona, S. Desportes, M. Altheimer, K. Ninck and P. R. Von Rohr, *Int. J. Heat Mass Transfer*, 2012, **55**, 522–530.
138 M. Liu, X. Zhu, Q. Liao, R. Chen, D. Ye and G. Chen, *Ind. Eng. Chem. Res.*, 2020, **59**, 9469–9477.
139 M. B. Plutschack, B. Pieber, K. Gilmore and P. H. Seeberger, *Chem. Rev.*, 2017, **117**, 11796–11893.
140 R. L. Hartman, J. P. McMullen and K. F. Jensen, *Angew. Chem., Int. Ed.*, 2011, **50**, 7502–7519.
141 K. Jähnisch, V. Hessel, H. Löwe and M. Baerns, *Angew. Chem., Int. Ed.*, 2004, **43**, 406–446.
142 M. Irfan, T. N. Glasnov and C. O. Kappe, *ChemSusChem*, 2011, **4**, 300–316.
143 C. H. Hornung, X. Nguyen, A. Carafa, J. Gardiner, A. Urban, D. Fraser, M. D. Horne, D. R. Gunasegaram and J. Tsanaktsidis, *Org. Process Res. Dev.*, 2017, **21**, 1311–1319.
144 S. Govender and H. B. Friedrich, *Catalysts*, 2017, **7**, 62.
145 V. Meille, *Appl. Catal., A*, 2006, **315**, 1–17.
146 S. Walter, S. Malmberg, B. Schmidt and M. A. Liauw, *Catal. Today*, 2005, **110**, 15–25.
147 E. V. Rebrov, G. B. F. Seijger, H. P. A. Calis, M. H. J. M. De Croon, C. M. Van Den Bleek and J. C. Schouten, *Appl. Catal., A*, 2001, **206**, 125–143.
148 M. Krivec, K. Žagar, L. Suhadolnik, M. Čeh and G. Dražić, *ACS Appl. Mater. Interfaces*, 2013, **5**, 9088–9094.
149 M. Alkaabi, M. Mohamed, A. Almanea, M. Alshehhi, K. Farousha, A. Yusuf and G. Palmisano, *ACS Omega*, 2022, **7**, 8306–8313.
150 M. W. Losey, M. A. Schmnidt and K. F. Jensen, *Ind. Eng. Chem. Res.*, 2001, **40**, 2555–2562.
151 L. Sang, X. Feng, J. Tu, B. Xie, G. Luo and J. Zhang, *Chem. Eng. J.*, 2020, **393**, 124793.
152 L. Zhang and J. Yue, *Chemistry*, 2025, **7**, 29.
153 M. A. M. Gijs, F. Lacharme and U. Lehmann, *Chem. Rev.*, 2010, **110**, 1518–1563.
154 P. Lisk, E. Bonnot, M. T. Rahman, R. Pollard, R. Bowman, V. Degirmenci and E. V. Rebrov, *Chem. Eng. J.*, 2016, **306**, 352–361.
155 X. Nguyen, A. Carafa and C. H. Hornung, *Chem. Eng. Process.*, 2018, **124**, 215–221.
156 R. Legg, C. Zhang, M. Bourchier, S. Cole, I. Martinez-Botella, X. Nguyen, Y. Zhu, W. Liew, S. Saubern, J. Tsanaktsidis and C. H. Hornung, *Chem.-Ing.-Tech.*, 2022, **94**, 1017–1023.
157 D. Wu and H. Zhang, *Ind. Eng. Chem. Res.*, 2013, **52**, 14713–14721.
158 M. T. Kreutzer, F. Kapteijn, J. A. Moulijn and J. J. Heiszwolf, *Chem. Eng. Sci.*, 2005, **60**, 5895–5916.
159 C. Algieri, G. Coppola, D. Mukherjee, M. I. Shammas, V. Calabro, S. Curcio and S. Chakraborty, *Catalysts*, 2021, **11**, 691.
160 A. Arratibel Plazaola, D. A. Pacheco Tanaka, M. Van Sint Annaland and F. Gallucci, *Molecules*, 2017, **22**, 51.
161 R. L. Papurello, J. L. Fernández, E. E. Miró and J. M. Zamaro, *Chem. Eng. J.*, 2017, **313**, 1468–1476.
162 X. Huang, G. Zhang, L. Zhang and Q. Zhang, *ACS Omega*, 2020, **5**, 20784–20791.
163 D. Stein, M. Kruithof and C. Dekker, *Phys. Rev. Lett.*, 2004, **93**, 035901.
164 R. Hatsuki, F. Yujiro and T. Yamamoto, *Microfluid. Nanofluid.*, 2013, **14**, 983–988.
165 C. Lee, L. Joly, A. Siria, A.-L. Biance, R. Fulcrand and L. Bocquet, *Nano Lett.*, 2012, **12**, 4037–4044.

166 K. Morikawa, K. Mawatari, M. Kato, T. Tsukahara and T. Kitamori, *Lab Chip*, 2010, **10**, 871–875.
167 K. Morikawa and T. Tsukahara, *Colloid Interface Sci. Commun.*, 2022, **50**, 100646.
168 T. Tsukahara, A. Hibara, Y. Ikeda and T. Kitamori, *Angew. Chem., Int. Ed.*, 2007, **46**, 1180–1183.
169 H. Chinen, K. Mawatari, Y. Pihosh, K. Morikawa, Y. Kazoe, T. Tsukahara and T. Kitamori, *Angew. Chem., Int. Ed.*, 2012, **51**, 3573–3577.
170 K. Morikawa, K. Mawatari, Y. Kazoe, T. Tsukahara and T. Kitamori, *Appl. Phys. Lett.*, 2011, **99**, 123115.
171 K. Morikawa, C.-C. Chang and Y. Kazoe, *Colloids Surf., A*, 2025, **719**, 137036.
172 T. Tsukahara, K. Nagaoka, K. Morikawa, K. Mawatari and T. Kitamori, *J. Phys. Chem. B*, 2015, **119**, 14750–14755.
173 K. Morikawa, Y. Kazoe, K. Mawatari, T. Tsukahara and T. Kitamori, *Anal. Chem.*, 2015, **87**, 1475–1479.
174 Y. Xu and B. Xu, *Small*, 2015, **11**, 6165–6171.
175 Y. Kazoe, S. Kubori, K. Morikawa, K. Mawatari and T. Kitamori, *Anal. Sci.*, 2022, **38**, 281–287.
176 Y. Kazoe, K. Ikeda, K. Mino, K. Morikawa, K. Mawatari and T. Kitamori, *Anal. Sci.*, 2023, **39**, 779–784.